

Fracton Self-Statistics

Hao Song,^{1,2} Nathanan Tantivasadakarn,^{3,4,5} Wilbur Shirley,^{6,4,7} and Michael Hermele⁸

¹CAS Key Laboratory of Theoretical Physics, Institute of Theoretical Physics, Chinese Academy of Sciences, Beijing 100190, China

²Department of Physics and Astronomy, McMaster University, Hamilton, Ontario L8S 4M1, Canada

³Walter Burke Institute for Theoretical Physics, California Institute of Technology, Pasadena, CA 91125, USA

⁴Department of Physics, California Institute of Technology, Pasadena, CA 91125, USA

⁵Department of Physics, Harvard University, Cambridge, MA 02138, USA

⁶School of Natural Sciences, Institute for Advanced Study, Princeton, NJ 08540, USA

⁷Institute for Quantum Information and Matter, California Institute of Technology, Pasadena, CA 91125, USA

⁸Department of Physics and Center for Theory of Quantum Matter, University of Colorado, Boulder, CO 80309, USA

(Dated: March 29, 2024)

Fracton order describes novel quantum phases of matter that host quasiparticles with restricted mobility, and thus lies beyond the existing paradigm of topological order. In particular, excitations that cannot move without creating multiple excitations are called fractons. Here we address a fundamental open question—can the notion of self-exchange statistics be naturally defined for fractons, given their complete immobility as isolated excitations? Surprisingly, we demonstrate how fractons can be exchanged, and show that their self-statistics is a key part of the characterization of fracton orders. We derive general constraints satisfied by the fracton self-statistics in a large class of Abelian fracton orders. Finally, we show the existence of nontrivial fracton self-statistics in some twisted variants of the checkerboard model and Haah’s code, establishing that these models are in distinct quantum phases as compared to their untwisted cousins.

Introduction. Particle statistics is a fundamental aspect of quantum mechanics. While elementary particles that compose our universe must be either bosons or fermions due to the topological triviality of double exchanges in 3D space, emergent quasiparticles in 2D quantum many-body systems can exhibit anyonic statistics [1, 2], which are crucial for characterizing conventional topological order. Recently, the theoretical discovery of fracton order in 3D [3–9] has revealed a new situation where quasiparticles lack their usual freedom to move in space, calling for a reexamination of the notion of statistics [10–12].

Fracton systems have emerged as an active frontier of quantum physics [13, 14], attracting great interest from condensed matter, quantum information and quantum field theory viewpoints. Fracton order is defined by the emergence of quasiparticles with restricted mobility, including *fractons*, which cannot move without splitting into more than one excitation. Single isolated fractons are thus immobile. Fracton models can also host excitations which are mobile only within planes or lines. Statistical processes involving or interpretable in terms of partially mobile excitations have been studied [10–12, 15–23]. Moreover, fractons can be non-Abelian in the sense of carrying protected topological degeneracy [11, 16, 24–35]. Nevertheless, a fundamental question remains open: does a notion of self-exchange statistics make sense for fractons, given their complete immobility as isolated excitations?

In this Letter, we provide a resolution to this puzzle. By allowing the fracton quasiparticle to split into multiple coordinated pieces, it is possible to prepare two well-separated realizations of the same fracton superselection sector. Such a pair of excitation patterns can be physically exchanged, giving rise to a fracton self-statistics. Our findings apply to both fracton phases of foliated [36, 37] and fractal [5, 6] nature. Furthermore, we point out instances where the self-statistics of fractons is in fact the only known statistical invariant that

distinguishes between two fracton phases. We provide explicit examples by distinguishing twisted checkerboard models [11] and a twisted Haah’s code [38] from their untwisted counterparts. Thus, we show that fracton self-statistics is a fundamental invariant needed to characterize fracton phases of matter.

Foliated fractons. To illustrate the principle, we start with the simplest relevant setting, in which all fractons a are Abelian [39] and satisfy the fusion constraint

$$a \times \overline{t_{\mu} a} \times t_{\nu} a \times \overline{t_{\nu} a} = 1 \quad (1)$$

for all $\mu, \nu \in \{x, y, z\}$ such that $\mu \neq \nu$, where $t_{\mu(\nu)}$ is the elementary lattice vector in the μ (ν) direction, $t_{\mu} a$ denotes the analogue of a at a t -shifted position, and $\overline{t_{\nu} a}$ is the antiparticle of $t_{\nu} a$. This constraint guarantees the existence of rectangular [40] membrane operators of arbitrary size that generate quadrupolar configurations of a given species a at its corners. Fractons satisfying the fusion constraint will be referred to as (Abelian) *foliated*.

A large body of models hosting foliated fractons are known in the literature, including the X-cube, checkerboard, and their many variants [8, 11, 17, 41–43]. Let us refer to the checkerboard model as a concrete example, for its twisted variants will clearly demonstrate the usage of fracton self-statistics.

The *checkerboard model* [8] is defined on a 3D checkerboard lattice (Fig. 1a) with one qubit per vertex v . Its Hamiltonian

$$H_{\text{cb}} = - \sum_c (A_c + B_c) \quad (2)$$

is a summation over gray cubes c in Fig. 1(a), where

$$A_c := \prod_{v \in c} X_v, \quad B_c := \prod_{v \in c} Z_v, \quad (3)$$

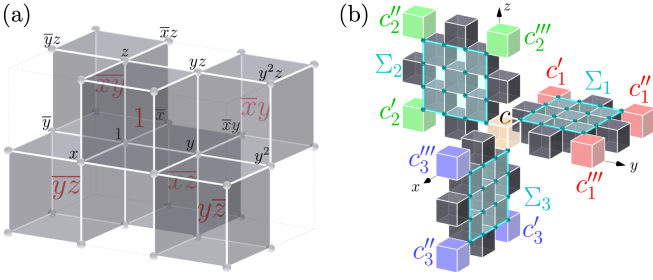


Figure 1. (a) 3D checkerboard lattice with vertices and gray cubes labeled by monomials $x^j y^k z^l$, where $\bar{x} \equiv x^{-1}$ etc. (b) In the checkerboard model, excitation $A_c = -1$ (or $B_c = -1$) has fractional mobility $\{c\} \rightarrow \{c'_i, c''_i, c'''_i\}$, realizable by operator $M_i = \prod_{v \in \Sigma_i} Z_v$ (respectively, $M_i = \prod_{v \in \Sigma_i} X_v$) supported on rectangular membrane Σ_i , for $i = 1, 2, 3$.

are products of Pauli X or Z operators at the eight vertices of c . This is an exactly solvable gapped model with spectrum labeled by simultaneous eigenvalues $\{A_c, B_c = \pm 1\}$.

An isolated excitation $A_c = -1$ exemplifies a foliated fracton. It can be “moved” at the expense of fractionalizing into more than one excitation, e.g., $\eta = \{c\} \rightarrow \eta_i = \{c'_i, c''_i, c'''_i\}$ by a rectangular membrane operator; see Fig. 1(b). Therefore, the excitation patterns η_1 (red), η_2 (green), η_3 (blue), and η (orange) are all realizations of the same fracton superselection sector.

Self-statistics of foliated fractons. Generically, a foliated fracton a is characterized by a set of four self-statistical phases $\theta_a^{[xyz]}$, $\theta_a^{[x\bar{y}z]}$, $\theta_a^{[x\bar{y}\bar{z}]}$, and $\theta_a^{[xy\bar{z}]}$, each corresponding to a “windmill” self-exchange process.

The process corresponding to $\theta_a^{[xyz]}$ is depicted in Fig. 2. It begins with an excited state with a at the center of the windmill, in addition to a triplet of excitations denoted \widehat{a} that belongs to the same superselection sector as a . The process proceeds with a sequence of six membrane operators (Fig. 3a) whose total action exchanges a with \widehat{a} , returning to the starting state in such a way that all arbitrary phases cancel. It can be regarded as a fractonic generalization of the T-shaped anyon exchange process [44].

The processes for $\theta_a^{[x\bar{y}z]}$, $\theta_a^{[x\bar{y}\bar{z}]}$, and $\theta_a^{[xy\bar{z}]}$ are defined analogously, but along windmills related to $[xyz]$ by a 180° -rotation about the x , y , and z axes, respectively. For instance, the $[x\bar{y}\bar{z}]$ process involves the membrane operators located as in Fig. 3(b). The notation $[\mu_1 \mu_2 \mu_3]$ of three directions μ_i refers to a windmill made of three blades $K_i = \text{cone}(-\mu_i, \mu_{i+1}) \equiv \{-\alpha \mu_i + \beta \mu_{i+1} | \alpha, \beta \geq 0\}$ for $i = 1, 2, 3$, where $\mu_4 \equiv \mu_1$. Each overlined direction indicates its opposite (e.g., $\bar{x} = -x$).

Although more windmill processes can be considered, they yield *no* new self-statistical phases beyond the four already defined. Any two inversion-related windmills (e.g., $[xyz]$ and $[x\bar{y}\bar{z}]$ in Fig. 3(a) and (c)) specify the same self-statistics. The reason is demonstrated in Fig. 3(d): membrane operators for $[xyz]$ and $[x\bar{y}\bar{z}]$ can be related by a deformation [45]. Consequently, despite eight possible windmill choices (see SM [46]), only four self-statistics need to be specified for fo-

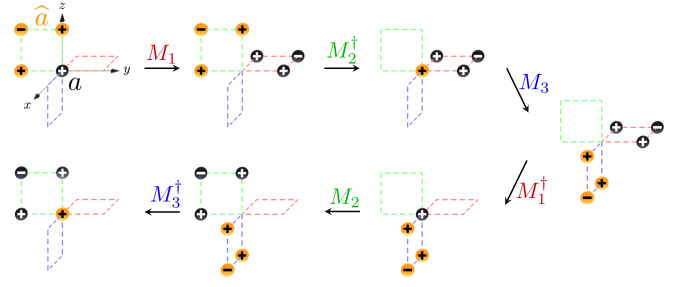


Figure 2. The $[xyz]$ windmill process. The starting state has an excitation a at the center of the “windmill”, along with three other excitations collectively called \widehat{a} in the same superselection sector as a following Eq. (1). The process involves three membrane operators M_1, M_2, M_3 , and their inverses, successively moving the four excitations from the corners of the yz square, to the corners of the zx square, and finally back to the original configuration. The process is designed such that the phase arbitrariness in the choice of M_i is precisely cancelled by the action of M_i^\dagger . Therefore, the universal statistical phase is well-defined by $\theta_a^{[xyz]} = M_3^\dagger M_2 M_1^\dagger M_3 M_2^\dagger M_1$.

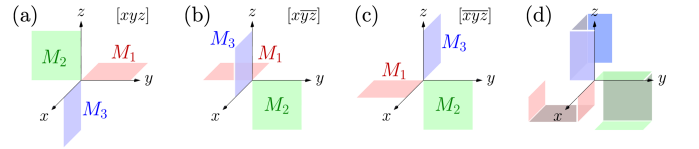


Figure 3. Membrane operators comprising the (a) $[xyz]$, (b) $[x\bar{y}z]$, and (c) $[x\bar{y}\bar{z}]$ windmill processes. (d) The membrane operators for the $[x\bar{y}\bar{z}]$ process are smoothly deformed such that, near the origin, they coincide with those of the $[xyz]$ process. This proves $\theta_a^{[x\bar{y}\bar{z}]} \equiv \theta_a^{[xyz]}$.

liated fractons.

One might expect that $\theta_a^{[xyz]}$, $\theta_a^{[x\bar{y}z]}$, $\theta_a^{[x\bar{y}\bar{z}]}$, and $\theta_a^{[xy\bar{z}]}$ are independent. To the contrary, they are subject to a constraint

$$\theta_a^{[xyz]} \theta_a^{[x\bar{y}z]} \theta_a^{[x\bar{y}\bar{z}]} \theta_a^{[xy\bar{z}]} = 1, \quad (4)$$

leaving only three of them independent in general.

This constraint is most naturally derived by utilizing a quantity S_{ab}^μ for $\mu = x, y, z$, defined as the mutual braiding statistics between dipoles $a \times \overline{l_\mu a}$ and $b \times \overline{-l_\mu b}$ in the large l limit. The dipoles are planons (i.e., quasiparticles mobile in two directions). The braiding direction is fixed by μ via the right hand rule. See Fig. 4(a).

A proof of Eq. (4) is as follows. If a is exchanged twice with \widehat{a} , both sets of excitations return to their original position. The total process is smoothly deformable into one where a is stationary while \widehat{a} braids around a . For instance, we can deform the $[x\bar{y}\bar{z}]$ windmill process into one along the cyclic “path” in Fig. 4(b). Similarly, the $[x\bar{y}\bar{z}]$ process (which produces statistics $\theta_a^{[x\bar{y}\bar{z}]} \equiv \theta_a^{[xyz]}$) is deformable into the one depicted in Fig. 4(c). If the two deformed exchanges are started and ended with the intermediate state containing excitations a and \widehat{a} , their composite gives the process in Fig. 4(d), implying

$$\theta_a^{[xyz]} \theta_a^{[x\bar{y}\bar{z}]} = S_{aa}^x. \quad (5)$$

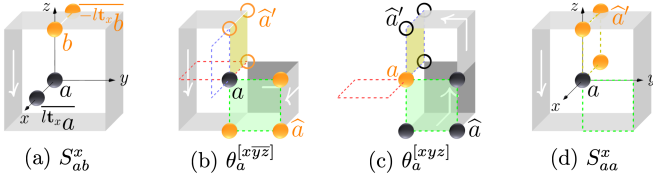


Figure 4. Graphic proof of $\theta_a^{[xy\bar{z}]} \theta_a^{[xyz]} = S_{aa}^x$. The white arrows denote the direction of braiding and exchange processes. (a) Definition of S_{ab}^x . (b) The $[xy\bar{z}]$ process (dotted windmill) is deformable into one realized in three steps $a \rightarrow \tilde{a}$, $\tilde{a} \rightarrow a$, and $\tilde{a}' \rightarrow \hat{a}$ using operators supported on the olive, green, and gray areas. The intermediate state \tilde{a} consists of excitations at the three circles. (c) A process which is equivalent to the $[xy\bar{z}]$ process and hence produces statistics $\theta_a^{[xy\bar{z}]} \equiv \theta_a^{[xyz]}$. (d) A process that braids part of \tilde{a}' , along on the gray ribbon, around a . The statistical phase due to the presence of a is S_{aa}^x .

Armed with this relation, we can now prove Eq. (4) by a 180-rotation of Eq. (5) about the y axis to obtain $\theta_a^{[xy\bar{z}]} \theta_a^{[xyz]} = (S_{aa}^x)^*$, and multiplying it with Eq. (5).

The mutual statistics also appear in the following formula for the self-statistics of a fusion product of two fractons, and analogous formulas due to cubic symmetry:

$$\theta_{a \times b}^{[xyz]} = \theta_a^{[xyz]} \theta_b^{[xyz]} S_{ab}^x S_{ab}^y S_{ab}^z. \quad (6)$$

See SM [46] for a proof. This relation implies

$$S_{ab}^x S_{ab}^y S_{ab}^z = S_{ba}^x S_{ba}^y S_{ba}^z. \quad (7)$$

It is interesting to note that Eqs. (5) and (6) generalize the constraints $\theta_a^2 = S_{aa}$ and $\theta_{a \times b} = \theta_a \theta_b S_{ab}$ of 2D Abelian topological orders, where θ_a is the topological spin and S the topological S -matrix. For an Abelian planon a satisfying the foliation condition Eq. (1), analogous windmill processes are reducible into 2D braidings and the above discussions reduce to these familiar 2D equations.

Now assume a foliated fracton satisfies $a^N = 1$. We show its self-statistics being constrained to *discrete* values for use in distinguishing fracton orders. Note $S_{aa}^x S_{aa}^y S_{aa}^z = (\theta_a^{[xyz]})^2$ by virtue of Eqs. (4) and (5). Thus, since $(S_{aa}^\mu)^N = S_{a^N a}^\mu = 1$, we have $(\theta_a^{[xyz]})^{2N} = 1$. Moreover, applying Eq. (6) recursively gives $(\theta_a^{[xyz]})^{N^2} = \theta_{a^N}^{[xyz]} = 1$. Together, these imply the self-statistics of a being multiples of $e^{2\pi i / (N \gcd(N, 2))}$ in analogy to anyons in 2D.

Semionic fractons in twisted checkerboard models. A major application of fracton self-statistics is to distinguish the quantum phase of the checkerboard model H_{cb} from its twisted variants introduced in Ref. [11]. To illustrate, we consider seven twisted models, denoted $H_{cb}^x, H_{cb}^y, H_{cb}^z, H_{cb}^{xy}, H_{cb}^{yz}, H_{cb}^{zx}$, and H_{cb}^{xyz} below. Together with H_{cb} , we will show that the eight models fall into two quantum phases, distinguishable by the presence or absence of semionic fracton self-statistics. Explicit construction of paths connecting models with identical fracton self-statistics is given in SM [46].

First, in H_{cb} (Eq. (2)), all excitations (including fractons) exhibit either bosonic (+1) or fermionic (-1) statistics. This is

because all statistical processes are realizable by tensor products of Pauli operators which only commute or anticommute with each other.

In contrast, H_{cb}^x represents a new phase allowing *semionic* ($\pm i$) fracton self-statistics. Instead of using the formalism in Ref. [11], we specify this model using a non-Pauli stabilizer Hamiltonian

$$H_{cb}^x = - \sum_c (A_c^x + B_c) \quad (8)$$

obtained by replacing A_c in the untwisted model Eq. (2) with a modified term A_c^x , to have a convenient description of excitations with $(A_c^x)^2 = 1$ and the full spectrum labeled by simultaneous eigenvalues $\{A_c^x, B_c = \pm 1\}$, where x refers to twisting being associated with x -edges. Explicitly, we label vertices and cubes by monomials as in Fig. 1(a) and denote finite sets of vertices by polynomials with $\mathbb{Z}_2 = \{0, 1\}$ coefficients [47]. In this notation,

$$A_c^x := A_c \phi_{(1+x)\bar{x}c} \phi_{(1+x)xc} \quad (9)$$

according to the construction described in SM [46], where $\ell = (1+x)\bar{x}c$ and $\ell = (1+x)xc$ denote vertex pairs that are ends of x -edges, and

$$\phi_\ell := (-1)^{n_{\bar{y}}^- n_{\bar{z}}^- + n_{\bar{y}z}^- n_{\bar{z}}^- + n_{\bar{z}}^- n_{\bar{y}}^+ + n_{\bar{z}}^- n_{\bar{y}z}^+ + n_{\bar{y}}^+ n_{\bar{z}}^+ + n_{\bar{y}z}^+ n_{\bar{z}}^+ + n_{\bar{y}z}^+ n_{\bar{z}}^+} \cdot (-1)^{n_{\bar{y}z}^-(1+y) n_{\bar{y}z}^-(1+y)(1+z)} \cdot i^{-n_{\bar{z}}^-(1+y)(1+z)} \quad (10)$$

is a Dijkgraaf-Witten twisting factor, with the shorthand

$$Z_\kappa := \prod_{v \in \kappa} Z_v, \quad n_\kappa^\pm := \frac{1}{2} (1 \pm Z_\kappa), \quad (11)$$

for κ any finite set of vertices.

In H_{cb}^x , one example of semionic fracton is a $B_c = -1$ excitation (denoted m_x below), which has

$$\theta_{m_x}^{[xyz]} = \theta_{m_x}^{[xy\bar{z}]} = i \quad \text{and} \quad \theta_{m_x}^{[x\bar{y}z]} = \theta_{m_x}^{[x\bar{y}\bar{z}]} = -i. \quad (12)$$

Two derivations of the statistics are given in SM [46]. In one, we construct a modified X operator that explicitly generates the statistical processes for B excitations. The modification of X is required to ensure no A_c^x terms flipped, and results in the above semionic self-statistics.

We emphasize that in H_{cb}^x , exotic self-statistics ($\theta \neq \pm 1$) are exclusive to fractons. Ref. [11] reported that non-fractonic excitations in H_{cb}^x exhibit only bosonic or fermionic statistics. This implies that H_{cb}^x cannot be a tensor product of H_{cb} and 2D anyon models containing semions. Therefore, the fact that only fracton self-statistics can distinguish the two models highlights the novelty of H_{cb}^x as a distinct phase of matter. We refer to the phase of H_{cb}^x as a *semionic fracton order*, as characterized by the presence of semionic statistics for only the fracton excitations.

The remaining six models are constructed similarly to H_{cb}^x . In H_{cb}^x , the twisting factor $\phi_{(1+x)\bar{x}c} \phi_{(1+x)xc}$ in Eq. (9) is linked to

x -edges. Its analogue associated with y -edges (z -edges) specifies H_{cb}^y (H_{cb}^z). Moreover, twisting can be applied to more than one direction simultaneously; for example, H_{cb}^{xy} has twisting made along both x -edges and y -edges.

Remarkably, despite the six models having different ground states, we discover that: (1) H_{cb}^y , H_{cb}^z , and H_{cb}^{xyz} represent the same semionic fracton phase as H_{cb}^x , while (2) H_{cb}^{xy} , H_{cb}^{yz} , and H_{cb}^{zx} fall within the phase of H_{cb} . Let us first demonstrate how fracton self-statistics are matched between H_{cb}^{xy} and H_{cb} . In H_{cb}^{xy} , excitation $B_c = -1$ (denoted m_{xy}) is a fracton with

$$\begin{aligned} \theta_{m_{xy}}^{[xyz]} &= i \cdot i = -1, & \theta_{m_{xy}}^{[\bar{x}y\bar{z}]} &= (-i)^2 = -1, \\ \theta_{m_{xy}}^{[x\bar{y}z]} &= i \cdot (-i) = 1, & \theta_{m_{xy}}^{[\bar{x}\bar{y}z]} &= (-i) \cdot i = 1, \end{aligned} \quad (13)$$

where two twistings cause a cancellation in semionic character. Further, combining m_{xy} with an A excitation at relative position $\bar{x}y$, denoted $\bar{x}y e$, yields a fracton $\bar{x}y e \times m_{xy}$ with purely bosonic self-statistics, which can be seen via Eq. (6) and its analogues.

Based on this observation, we indeed find an exact local unitary transformation relating the ground states of H_{cb}^{xy} and H_{cb} , rigorously confirming they represent the same phase (see SM [46]). Other phase identifications in the classification can be proven analogously.

Self-statistics of fractal fractons. The notion of self-statistics extends to non-foliated fractons [48]. We demonstrate this with Haah’s code [5]

$$H_{\text{Haah}} = - \sum_{\lambda \in \Lambda} (A_\lambda + B_\lambda), \quad (14)$$

an exactly solvable model defined on a cubic lattice with two qubits per vertex. Here, $\Lambda = \{x^i y^j z^k\}$ represents lattice vectors $(i, j, k) \in \mathbb{Z}^3$ in monomial form. The A (B) terms are translations of the representative A_1 (B_1) at the origin given in Fig. 5(a). Each A_λ (B_λ) is a product of eight Pauli X ’s (Z ’s). With collections of translationally related objects represented as sums of Λ ’s elements, we can describe A_λ and B_λ using Laurent polynomials with $\mathbb{Z}_2 = \{0, 1\}$ coefficients [47]:

$$A_\lambda = \lambda \cdot (\bar{f}_1, \bar{f}_2, 0, 0), \quad B_\lambda = \lambda \cdot (0, 0, f_2, f_1), \quad (15)$$

$$f_1 = 1 + x + y + z, \quad f_2 = 1 + xy + yz + zx, \quad (16)$$

$$\bar{f}_1 = 1 + \bar{x} + \bar{y} + \bar{z}, \quad \bar{f}_2 = 1 + \bar{x}\bar{y} + \bar{y}\bar{z} + \bar{z}\bar{x}. \quad (17)$$

where the first (last) two components of A_λ and B_λ locate Pauli X ’s (Z ’s) for the two qubit species. The bar denotes spatial inversion: $x \rightarrow \bar{x} \equiv x^{-1}$ etc.

Excitations can also be described by polynomials. Applying a Pauli Z to the first (or second) qubit at the origin excites A -terms in the pattern f_1 (respectively, f_2). Interestingly, one may flip A -terms purely in the yz plane [6] by noting

$$(y + z)f_1 + f_2 = 1 + y + y^2 + z + yz + z^2 =: g. \quad (18)$$

Consider planar fractional moves for visual clarity. The yz -planar ones are generated by g , allowing A excitations to travel arbitrarily long distances toward each of the *conic* directions

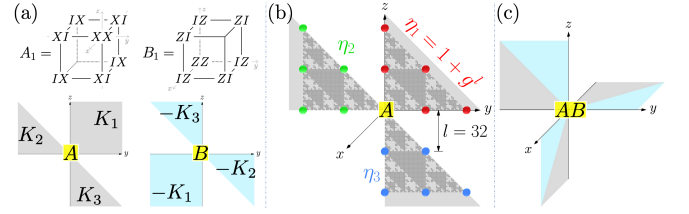


Figure 5. Fracton’s mobility in the Haah’s code. (a) Top: definition of A_1 and B_1 . They are products of eight Pauli’s. Identity operators I are omitted when possible. Bottom: mobility cones (on the yz -plane) for A and B excitations. (b) Fractional moves $1 \rightarrow \eta_i$ of an A excitation are realized by operators of fractal support. Gray square dots represent operator $(0, 0, y + z, 1)$ and its translations. (c) A windmill for a composite of type- A and type- B fractons.

K_1 , K_2 , and K_3 in Fig. 5(a). Explicitly, for $l = 2^n$, one has $1 + g^l = y^l + y^{2l} + z^l + z^{2l}y^l + z^{2l}$ due to the \mathbb{Z}_2 setting of the model. Accordingly, $1 \rightarrow 1 + g^l$ provides an instance of pushing an A -term excitation by at least l distance toward K_1 . It is realizable by fractal-shaped operator $g^{l-1}(0, 0, y + z, 1)$, reflecting the excitation being a fracton of fractal nature. See Fig. 5(b). We call each K_i a *mobility cone* for A excitations, as defined in SM [46]. The description of B excitations are analogous but with spatial directions inverted.

Based on mobility cones, we categorize fractons of H_{Haah} into three types— A , B , and mixed—and define their windmill self-statistical processes. Type- A (type- B) are fractons with the mobility cones K_i (respectively, $-K_i$) for $i = 1, 2, 3$ shown in Fig. 5(a). The mixed are bound states of type- A and type- B ; they cannot be moved along any individual cone among K_i ’s or $-K_i$ ’s. Self-statistics is definable using the “windmill” made of mobility cones. See Figs. 5(a) and (c). In H_{Haah} , non-mixed (i.e., type- A or type- B) fractons exhibit purely bosonic self-statistics, since only one type of Pauli is involved.

Fermionic type- A fractons in a twisted Haah’s code. To further illustrate the usage of fracton self-statistics, consider a gauge-theoretic variant of Haah’s code defined by applying H_{Haah} to a Hilbert space that binds a *fermionic* mode ψ_λ to A_λ via Gauss’s law $-i\gamma_\lambda \tilde{\gamma}_\lambda A_\lambda = 1$, where $\gamma_\lambda := \psi_\lambda + \psi_\lambda^\dagger$ and $\tilde{\gamma}_\lambda := \frac{1}{i}(\psi_\lambda - \psi_\lambda^\dagger)$ are Majorana operators. As detailed in SM [46], the gauge theory emerges from a spin model H_{Haah}^F , namely, the twisted Haah’s code proposed in Ref. [38].

Fracton self-statistics enables us to settle the unresolved question of whether H_{Haah}^F represents a distinct fracton order from the original Haah’s code H_{Haah} . The expectation that A excitation becomes fermionic is now definable and provable via windmill processes. The operator creating A -excitations is modified to $Z_\sigma c_\sigma$ due to gauge invariance, where Z_σ denotes Pauli Z on qubit σ while c_σ denotes a product of γ_λ ’s that are associated with the Z_σ -flipped A terms. Still, one may wonder whether it is possible to compensate the statistics change by attaching B excitations to A . Indeed, this is the case for the 2D toric code, and the checkerboard model, which we have shown above. However, it is not allowed here because attaching type- B fractons alters the mobility of A . Thus,

the presence of fermionic type-*A* fractons distinguishes H_{Haah}^F from H_{Haah} . See also SM [46] for the discreteness of this self-statistics, which confirms the phase distinction.

Conclusions. We have shown that it is possible to exchange two realizations of a fracton superselection sector via its fractional mobility. The notion of self-statistics for fractons can thus be introduced, which is essential in characterizing fracton orders. As applications, we studied a family of twisted checkerboard models and a twisted Haah’s code, from which we revealed a novel phase of foliated nature—what we call a semionic fracton order—and a new fractal-type order characterized by emergent fermionic fractons. Our work marks a crucial step towards a full “algebraic theory of fractons” yet to be developed.

We thank Sheng-Jie Huang, Juven Wang and especially Ashvin Vishwanath for helpful discussions. The authors are grateful to the Banff International Research Station, where this work began in 2020 at the workshop “Fractons and Beyond.” HS also acknowledges discussions with Sung-Sik Lee. HS has been supported by the Natural Sciences and Engineering Research Council of Canada and the National Natural Science Foundation of China (Grant No. 12047503). NT is supported by the Walter Burke Institute for Theoretical Physics at Caltech. The work of MH is supported by the U.S. Department of Energy, Office of Science, Basic Energy Sciences (BES) under Award number DE-SC0014415. WS is supported by the Simons Collaboration on Ultra-Quantum Matter (UQM), which is a grant from the Simons Foundation (651444). The work of NT, WS and MH also benefited from meetings of the UQM Simons Collaboration supported by Simons Foundation grant number 618615.

-
- [1] Daniel Arovas, J. R. Schrieffer, and Frank Wilczek, “Fractional statistics and the quantum hall effect,” *Phys. Rev. Lett.* **53**, 722–723 (1984).
- [2] Alexei Kitaev, “Anyons in an exactly solved model and beyond,” *Annals of Physics* **321**, 2–111 (2006), January Special Issue.
- [3] Claudio Chamon, “Quantum glassiness in strongly correlated clean systems: An example of topological overprotection,” *Phys. Rev. Lett.* **94**, 040402 (2005).
- [4] Sergey Bravyi, Bernhard Leemhuis, and Barbara M. Terhal, “Topological order in an exactly solvable 3d spin model,” *Annals of Physics* **326**, 839–866 (2011).
- [5] Jeongwan Haah, “Local stabilizer codes in three dimensions without string logical operators,” *Phys. Rev. A* **83**, 042330 (2011).
- [6] Beni Yoshida, “Exotic topological order in fractal spin liquids,” *Phys. Rev. B* **88**, 125122 (2013).
- [7] Sagar Vijay, Jeongwan Haah, and Liang Fu, “A new kind of topological quantum order: A dimensional hierarchy of quasiparticles built from stationary excitations,” *Phys. Rev. B* **92**, 235136 (2015).
- [8] Sagar Vijay, Jeongwan Haah, and Liang Fu, “Fracton topological order, generalized lattice gauge theory, and duality,” *Phys. Rev. B* **94**, 235157 (2016), arXiv:1603.04442.
- [9] Michael Pretko, “Subdimensional particle structure of higher rank $u(1)$ spin liquids,” *Phys. Rev. B* **95**, 115139 (2017).
- [10] Han Ma, Ethan Lake, Xie Chen, and Michael Hermele, “Fracton topological order via coupled layers,” *Phys. Rev. B* **95**, 245126 (2017).
- [11] Hao Song, Abhinav Prem, Sheng-Jie Huang, and M. A. Martin-Delgado, “Twisted fracton models in three dimensions,” *Phys. Rev. B* **99**, 155118 (2019), arXiv:1805.06899.
- [12] Shriya Pai and Michael Hermele, “Fracton fusion and statistics,” *Phys. Rev. B* **100**, 195136 (2019).
- [13] Rahul M. Nandkishore and Michael Hermele, “Fractons,” *Annual Review of Condensed Matter Physics* **10**, 295–313 (2019).
- [14] Michael Pretko, Xie Chen, and Yizhi You, “Fracton phases of matter,” *International Journal of Modern Physics A* **35**, 2030003 (2020).
- [15] Kevin Slagle and Yong Baek Kim, “Quantum field theory of x -cube fracton topological order and robust degeneracy from geometry,” *Phys. Rev. B* **96**, 195139 (2017).
- [16] Sagar Vijay and Liang Fu, “A generalization of non-abelian anyons in three dimensions,” (2017), arXiv:1706.07070.
- [17] Abhinav Prem, Sheng-Jie Huang, Hao Song, and Michael Hermele, “Cage-net fracton models,” *Phys. Rev. X* **9**, 021010 (2019).
- [18] Wilbur Shirley, Kevin Slagle, and Xie Chen, “Fractional excitations in foliated fracton phases,” *Annals of Physics* **410**, 167922 (2019).
- [19] Daniel Bulmash and Thomas Iadecola, “Braiding and gapped boundaries in fracton topological phases,” *Phys. Rev. B* **99**, 125132 (2019).
- [20] Yizhi You, Trihep Devakul, F.J. Burnell, and S.L. Sondhi, “Symmetric fracton matter: Twisted and enriched,” *Annals of Physics* **416**, 168140 (2020).
- [21] Wilbur Shirley, “Fractonic order and emergent fermionic gauge theory,” (2020), arXiv:2002.12026.
- [22] Nathanan Tantivasadakarn, Wenjie Ji, and Sagar Vijay, “Hybrid fracton phases: Parent orders for liquid and nonliquid quantum phases,” *Phys. Rev. B* **103**, 245136 (2021).
- [23] Wilbur Shirley, Xu Liu, and Arpit Dua, “Emergent fermionic gauge theory and foliated fracton order in the chamon model,” *Phys. Rev. B* **107**, 035136 (2023).
- [24] Daniel Bulmash and Maissam Barkeshli, “Gauging fractons: Immobile non-abelian quasiparticles, fractals, and position-dependent degeneracies,” *Phys. Rev. B* **100**, 155146 (2019).
- [25] Abhinav Prem and Dominic J. Williamson, “Gauging permutation symmetries as a route to non-Abelian fractons,” *SciPost Phys.* **7**, 68 (2019).
- [26] Juven Wang and Kai Xu, “Higher-rank tensor field theory of non-abelian fracton and embeddon,” *Annals of Physics* **424**, 168370 (2019).
- [27] Juven Wang, Kai Xu, and Shing-Tung Yau, “Higher-rank tensor non-abelian field theory: Higher-moment or subdimensional polynomial global symmetry, algebraic variety, noether’s theorem, and gauging,” *Phys. Rev. Research* **3**, 013185 (2021).
- [28] Juven Wang and Shing-Tung Yau, “Non-abelian gauged fracton matter field theory: Sigma models, superfluids, and vortices,” *Phys. Rev. Research* **2**, 043219 (2020).
- [29] David Aasen, Daniel Bulmash, Abhinav Prem, Kevin Slagle, and Dominic J. Williamson, “Topological defect networks for fractons of all types,” *Phys. Rev. Research* **2**, 043165 (2020).
- [30] Xiao-Gang Wen, “Systematic construction of gapped nonliquid states,” *Phys. Rev. Research* **2**, 033300 (2020).
- [31] Juven Wang, “Nonliquid cellular states: Gluing gauge-higher-symmetry-breaking versus gauge-higher-symmetry-extension interfacial defects,” *Phys. Rev. Res.* **4**, 023258 (2022).

- [32] Dominic J. Williamson and Meng Cheng, “Designer non-abelian fractons from topological layers,” *Phys. Rev. B* **107**, 035103 (2023).
- [33] David T. Stephen, José Garre-Rubio, Arpit Dua, and Dominic J. Williamson, “Subsystem symmetry enriched topological order in three dimensions,” *Phys. Rev. Research* **2**, 033331 (2020).
- [34] Nathanan Tantivasadakarn, Wenjie Ji, and Sagar Vijay, “Non-abelian hybrid fracton orders,” *Phys. Rev. B* **104**, 115117 (2021).
- [35] Yi-Ting Tu and Po-Yao Chang, “Non-abelian fracton order from gauging a mixture of subsystem and global symmetries,” *Phys. Rev. Res.* **3**, 043084 (2021).
- [36] Wilbur Shirley, Kevin Slagle, Zhenghan Wang, and Xie Chen, “Fracton models on general three-dimensional manifolds,” *Phys. Rev. X* **8**, 031051 (2018).
- [37] Zongyuan Wang, Xiuqi Ma, David T. Stephen, Michael Hermele, and Xie Chen, “Renormalization of ising cage-net model and generalized foliation,” *Phys. Rev. B* **108**, 035148 (2023).
- [38] Nathanan Tantivasadakarn, “Jordan-wigner dualities for translation-invariant hamiltonians in any dimension: Emergent fermions in fracton topological order,” *Phys. Rev. Research* **2**, 023353 (2020).
- [39] Non-Abelian generalizations will be studied in the future.
- [40] Generally, $\{x, y, z\}$ may be oblique axes and accordingly membranes are parallelogrammatic. However, for convenience, we assume $\{x, y, z\}$ to be orthogonal in this paper.
- [41] Yizhi You, Trithep Devakul, FJ Burnell, and SL Sondhi, “Symmetric fracton matter: Twisted and enriched,” *Annals of Physics* **416**, 168140 (2020).
- [42] Wilbur Shirley, Kevin Slagle, and Xie Chen, “Twisted foliated fracton phases,” *Phys. Rev. B* **102**, 115103 (2020).
- [43] Trithep Devakul, Wilbur Shirley, and Juven Wang, “Strong planar subsystem symmetry-protected topological phases and their dual fracton orders,” *Phys. Rev. Res.* **2**, 012059 (2020).
- [44] See Fig. 10 of Ref. [2] for instance.
- [45] They are matched $(M_1, M_2, M_3)_{\lfloor xy\bar{z} \rfloor} \sim (M_3, M_1, M_2)_{\lfloor x\bar{y}z \rfloor}$ up to a permutation, leaving self-statistics unchanged.
- [46] See Supplementary Material for the counting of windmills for foliated fractons, a proof of Eq. (6), details of twisted checkerboard models, a mathematical treatment of mobility cones, details of the twisted Haah’s code, and the discreteness of fracton self-statistics in both the phases of the Haah’s code and its twisted variant.
- [47] Jeongwan Haah, “Commuting pauli hamiltonians as maps between free modules,” *Communications in Mathematical Physics* **324**, 351–399 (2013).
- [48] Different fractional mobility structures impose distinct constraints on fracton statistics. The interplay will be interesting for future studies.
- [49] G Dauphinais, L Ortiz, S Varona, and M A Martin-Delgado, “Quantum error correction with the semion code,” *New Journal of Physics* **21**, 053035 (2019).
- [50] Julio Carlos Magdalena de la Fuente, Nicolas Tarantino, and Jens Eisert, “Non-pauli topological stabilizer codes from twisted quantum doubles,” *Quantum* **5**, 398 (2021).
- [51] Han Yan, Kevin Slagle, and Andriy H. Nevidomskyy, “Y-cube model and fractal structure of subdimensional particles on hyperbolic lattices,” (2022), [arXiv:2211.15829](https://arxiv.org/abs/2211.15829).
- [52] Michael A. Levin and Xiao-Gang Wen, “String-net condensation: A physical mechanism for topological phases,” *Phys. Rev. B* **71**, 045110 (2005).
- [53] Yuting Hu, Yidun Wan, and Yong-Shi Wu, “Twisted quantum double model of topological phases in two dimensions,” *Phys. Rev. B* **87**, 125114 (2013).
- [54] Tyler D. Ellison, Yu-An Chen, Arpit Dua, Wilbur Shirley, Nathanan Tantivasadakarn, and Dominic J. Williamson, “Pauli stabilizer models of twisted quantum doubles,” *PRX Quantum* **3**, 010353 (2022).
- [55] The idea of non-Pauli stabilizer formalism was discussed in Ref. [49, 50]. Here we further add the expressions and properties of elementary string operators, which are not found in the literature but are useful for many purposes.
- [56] Xie Chen, Zheng-Cheng Gu, and Xiao-Gang Wen, “Local unitary transformation, long-range quantum entanglement, wave function renormalization, and topological order,” *Phys. Rev. B* **82**, 155138 (2010).
- [57] Stephen Boyd and Lieven Vandenberghe, *Convex optimization* (Cambridge university press, 2004).

Supplementary Material for “Fracton Self-Statistics”

Hao Song, Nathanan Tantivasadakarn, Wilbur Shirley, and Michael Hermele

This supplementary material contains: (S.I) the counting of windmills for foliated fractons, (S.II) a proof of Eq. (6), (S.III) a non-Pauli stabilizer formulation of 2D double semion model (as a preliminary for twisted checkerboard models), (S.IV) details of twisted checkerboard models and their classification, (S.V) a mathematical treatment of mobility cones, (S.VI) details of the twisted Haah’s code, and (S.VII) the discreteness of fracton self-statistics in the Haah’s code and its twisted variant.

S.I. COUNTING OF WINDMILLS FOR FOLIATED FRACTONS

In this section, we enumerate the windmills for foliated fractons. There are eight of them: the yz plane has four quadrants for placing M_2 , and one has two choices of M_1 and M_3 (along the xy and zx planes respectively) after fixing M_2 as depicted in Fig. 3(b) and (c) of the main text. Explicitly, they can be denoted as $[xyz]$, $[x\bar{y}\bar{z}]$, $[\bar{x}y\bar{z}]$, $[\bar{x}\bar{y}z]$, $[\bar{x}yz]$, $[x\bar{y}z]$, and $[xy\bar{z}]$. The last four are the spacial inversions of the first four.

It is important to note that, while windmill processes generally exist (as also observed in our study of Haah’s code), the numbers of windmills and independent statistics vary with the underline fracton mobility structure. Our enumeration targets foliated fractons as defined by the main text’s Eq. (1), deferring analogous exhaustive counts of fracton statistical processes in other scenarios (including the fractal cases and many other variants like those in Refs. [23, 51]) to future studies.

S.II. PROOF OF EQ. (6)

This section presents a proof for the main text’s Eq. (6).

To start, we observe that $\theta_{q \times q'}^{[xyz]} = \theta_q^{[xyz]} \theta_{q'}^{[xyz]}$ if q and q' are excitations separated in the $[111]$ direction. This is because $\theta_{q \times q'}^{[xyz]}$ can be realized as a composition of the $[xyz]$ processes for q and q' , which are realized on two parallel windmills that do *not* intersect with each other. See Fig. S1.

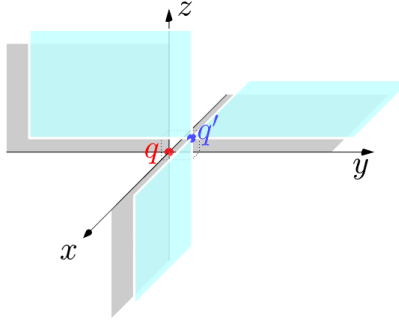


Figure S1. Illustration of $\theta_{q \times q'}^{[xyz]} = \theta_q^{[xyz]} \theta_{q'}^{[xyz]}$ for q and q' spatially separated in the $[111]$ direction.

Next, consider the $[xyz]$ self-statistics of $a \times b \times \overline{lm}a \times \overline{-lmb}$ for any large enough l , where $\mathbf{m} = \mathbf{t}_x + \mathbf{t}_y + \mathbf{t}_z$ denotes the $[111]$ direction. The above observation implies

$$\theta_{a \times b \times \overline{lm}a \times \overline{-lmb}}^{[xyz]} = \theta_{a \times b}^{[xyz]} \theta_{\overline{lm}a}^{[xyz]} \theta_{\overline{-lmb}}^{[xyz]}. \quad (\text{S1})$$

Similarly, for later use, we also have

$$\theta_{a \times \overline{lm}a}^{[xyz]} = \theta_a^{[xyz]} \theta_{\overline{lm}a}^{[xyz]} \quad \text{and} \quad \theta_{b \times \overline{-lmb}}^{[xyz]} = \theta_b^{[xyz]} \theta_{\overline{-lmb}}^{[xyz]}. \quad (\text{S2})$$

An alternate expression of the self-statistics of $a \times b \times \overline{lm}a \times \overline{-lmb}$ can be given in terms of statistics of $a \times \overline{lm}a$ and $b \times \overline{-lmb}$. To write it down explicitly, recall that, for each $\mu \in \{x, y, z\}$,

$$p_\mu^a := a \times \overline{t_\mu a} \quad \text{and} \quad p_\mu^b := b \times \overline{-t_\mu b} \quad (\text{S3})$$

are planons mobile in the directions perpendicular to μ . In particular, we have $p_y^a = a \times \overline{t_y a} = t_x a \times \overline{t_x + t_y a}$ and $p_z^a = a \times \overline{t_z a} = t_x + t_y a \times \overline{t_m a}$. Accordingly,

$$a \times \overline{t_m a} = a \times \overline{t_x a} \times t_x a \times \overline{t_x + t_y a} \times t_x + t_y a \times \overline{t_m a} = p_x^a \times p_y^a \times p_z^a. \quad (\text{S4})$$

Similarly, $b \times \overline{-t_m b} = p_x^b \times p_y^b \times p_z^b$. The associated windmill processes are thus reducible into braidings of planons. Therefore, $\theta_{a \times \overline{t_m a}}^{[xyz]} = \theta_{p_x^a} \theta_{p_y^a} \theta_{p_z^a}$, $\theta_{b \times \overline{-t_m b}}^{[xyz]} = \theta_{p_x^b} \theta_{p_y^b} \theta_{p_z^b}$, and more importantly, for our current purpose, $\theta_{a \times b \times \overline{t_m a} \times \overline{-t_m b}}^{[xyz]}$ can be expressed as

$$\theta_{a \times b \times \overline{t_m a} \times \overline{-t_m b}}^{[xyz]} = \theta_{a \times \overline{t_m a}}^{[xyz]} \cdot \theta_{b \times \overline{-t_m b}}^{[xyz]} \cdot S_{ab}^x S_{ab}^y S_{ab}^z, \quad (\text{S5})$$

where $\theta_{p_\mu^a(p_\mu^b)}$ is the braiding self-statistics of p_μ^a (p_μ^b) and S_{ab}^μ has been defined in the main text to be the mutual statistics between p_μ^a and p_μ^b .

Finally, the desired identity

$$\theta_{a \times b}^{[xyz]} = \theta_a^{[xyz]} \theta_b^{[xyz]} S_{ab}^x S_{ab}^y S_{ab}^z \quad (\text{S6})$$

is proven by comparing Eqs. (S1), (S2), and (S5).

S.III. NON-PAULI STABILIZER FORMULATION OF 2D DOUBLE SEMION MODEL

There are various ways to represent the 2D double semion phase [11, 49, 50, 52–54]. In this section, we turn a twisted gauge model for double semions into a non-Pauli stabilizer formalism [55], which will be used in Sec. S.IV to motivate the formulation of the twist checkerboard models used in the main text.

It is known that the double semion phase can be represented by a twisted \mathbb{Z}_2 gauge model [11, 53]. For the later convenience in making a comparison with layers of a 3D checkerboard, consider a 2D checkerboard with a physical qubit per vertex and triangulated as in Fig. S2(a), where the cyan regions (which we call *sites*) are left as holes for holding non-trivial fluxes. The formalism of 2D twisted gauge models [11] defines, for example, the flux term B_s and the gauge transformation \tilde{A}_s at site $s = 4$ as

$$B_4 := Z_{13} Z_{14} Z_{36} Z_{46}, \quad (\text{S7})$$

$$\begin{aligned} \tilde{A}_4 := & X_{14} X_{24} X_{46} X_{47} C(Z_{13}, Z_{14}) C(Z_{14}, -Z_{24}) C(-Z_{24}, Z_{25}) \\ & C(Z_{36}, Z_{46}) C(Z_{46}, -Z_{47}) C(-Z_{47}, Z_{57}) C(Z_{24} Z_{25}, B_5), \end{aligned} \quad (\text{S8})$$

where each edge (and the qubit on it) is labeled by its end sites, $B_5 := Z_{24} Z_{25} Z_{47} Z_{57}$ analogous to B_4 , and

$$C(P, Q) := (-1)^{\frac{1}{4}(1-P)(1-Q)} \quad (\text{S9})$$

is a shorthand for expressing controlled-Z gates and their generalizations.

The formalism of twisted gauge models ensures $[\tilde{A}_s, \tilde{A}_{s'}] = [\tilde{A}_s, B_{s'}] = [B_s, B_{s'}] = 0$. In addition, \tilde{A}_s corresponds to a projective representation of \mathbb{Z}_2 when $B_s = -1$. Explicitly, it is straightforward to check

$$\tilde{A}_s^2 = B_s \quad (\text{S10})$$

from the definition of \tilde{A}_s above. Consequently, $(\tilde{A}_s, B_s) = (1, 1), (-1, 1), (i, -1)$, and $(-i, -1)$ label the four possible states (with $(1, 1)$ being the trivial one) at each site s .

For convenience, replacing \tilde{A}_s with

$$\mathcal{A}_s := \tilde{A}_s (\sqrt{B_s})^\dagger \quad (\text{S11})$$

can turn this double semion model into a *non-Pauli stabilizer code*, where $\mathcal{A}_s^2 = B_s^2 = 1$, $[\mathcal{A}_s, \mathcal{A}_{s'}] = [\mathcal{A}_s, B_{s'}] = [B_s, B_{s'}] = 0$, and \mathcal{A}_s acts identically as \tilde{A}_s on the double semion ground states. The four states at s can thus be labeled by $(\mathcal{A}_s, B_s) = (1, 1), (-1, 1), (1, -1)$, and $(-1, -1)$. As shown below, their self-statistics are 1, 1, i , and $-i$ respectively.

First, $(\mathcal{A}_s, B_s) = (1, 1)$ denotes the absence of excitation and is hence trivial in all aspects (including self-statistics). Secondly, the self-statistics of $(\mathcal{A}_s, B_s) = (-1, 1)$ is also trivial; excitations of this type are created in pairs and moved by purely Pauli Z operators.

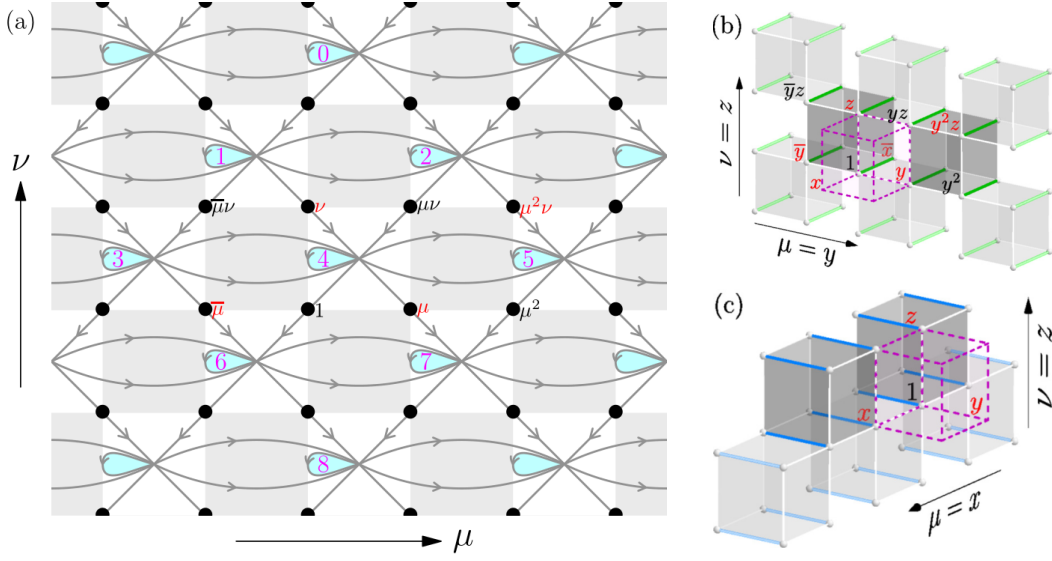


Figure S2. (a) A double semion model on a triangulated 2D checkerboard \mathcal{D} with a qubit per vertex (i.e., black dot). Cyan regions (which we call *sites*) are punched holes of the plane for holding fluxes. Operator \mathcal{A}_s for site $s = 4$ is supported on the eight qubits $\{\bar{\mu}, 1, \mu, \mu^2, \bar{\mu}\nu, \nu, \mu\nu, \mu^2\nu\}$, where $\bar{\mu} \equiv \mu^{-1}$. A label $\mu^j\nu^k$ is in red if $j+k$ is odd. (b) [respectively, (c)] A correspondence between an x -layer (y -layer) of 3D checkerboard and the 2D checkerboard \mathcal{D} , in which x -edges (y -edges), colored green (blue), correspond to the black dots of \mathcal{D} . Twisting this layer of the 3D checkerboard model adds, to the A term at the dashed magenta cube, a phase factor depending on the variables $Z_{v(1+x)} = Z_v Z_{vx}$ (respectively, $Z_{v(1+y)} = Z_v Z_{vy}$) associated with the x -edges (y -edges) of the two neighbor cubes shown in a darker gray. Vertex (i, j, k) is labeled $x^i y^j z^k$ and the label is shown in red (black) if $i+j+k$ is odd (even), where $\bar{x} \equiv x^{-1}$ etc.

As for $(\mathcal{A}_s, B_s) = (1, -1)$, let $\mathcal{S}_{ss'}$ be an operator flipping only B_s and $B_{s'}$ at the ends of edge $\langle ss' \rangle$. Physically, one may view $\mathcal{S}_{ss'}$ as an elementary string operator or as a modified bit-flip operator. It takes the form

$$\mathcal{S}_{24} := X_{14} \sqrt{Z_{24}} C(Z_{13}, Z_{14}) C(Z_{01} Z_{02}, Z_{14} Z_{24}) C(-Z_{13} Z_{14}, Z_{36} Z_{46}), \quad (\text{S12})$$

$$\mathcal{S}_{47} := X_{46} (\sqrt{Z_{47}})^\dagger C(Z_{36}, Z_{46}) C(Z_{13} Z_{14}, Z_{36} Z_{46}) C(-Z_{46} Z_{47}, Z_{68} Z_{78}) \quad (\text{S13})$$

for $\langle ss' \rangle = \langle 24 \rangle$ and $\langle 47 \rangle$, and is specified by translation symmetry in general. By direct computation, one has

$$\mathcal{S}_{ss'}^2 = B_s B_{s'}, \quad \mathcal{S}_{ss'}^\dagger = \mathcal{S}_{ss'} B_s B_{s'}, \quad [\mathcal{S}_{ss'}, \mathcal{S}_{s''s'''}] = 0 \text{ if } s, s', s'', \text{ and } s''' \text{ are four distinct sites}, \quad (\text{S14})$$

$$[\mathcal{S}_{ss'}, \mathcal{A}_{s''}] = 0, \quad \forall s'', \quad [\mathcal{S}_{ss'}, B_{s''}] = 0, \quad \forall s'' \neq s, s', \quad \{\mathcal{S}_{ss'}, B_s\} = \{\mathcal{S}_{ss'}, B_{s'}\} = 0, \quad (\text{S15})$$

$$\mathcal{S}_{s's} \mathcal{S}_{s''s} = i \mathcal{S}_{s''s} \mathcal{S}_{s's}, \quad \forall s'' \text{ is on the left of } s', \quad \text{e.g., } \mathcal{S}_{24} \mathcal{S}_{14} = i \mathcal{S}_{14} \mathcal{S}_{24}, \quad (\text{S16})$$

$$\mathcal{S}_{ss'} \mathcal{S}_{s''s'} = -i \mathcal{S}_{s''s'} \mathcal{S}_{ss'}, \quad \forall s'' \text{ is on the left of } s', \quad \text{e.g., } \mathcal{S}_{47} \mathcal{S}_{46} = -i \mathcal{S}_{46} \mathcal{S}_{47}, \quad (\text{S17})$$

$$\mathcal{S}_{ss'} \mathcal{S}_{s''s} = -\mathcal{S}_{s''s} \mathcal{S}_{ss'} B_s, \quad \text{e.g., } \mathcal{S}_{47} \mathcal{S}_{14} = -\mathcal{S}_{14} \mathcal{S}_{47} B_4, \quad (\text{S18})$$

where all edges are assumed oriented as in Fig. S2(a). A generic string operator for $(\mathcal{A}_s, B_s) = (1, -1)$ can be written as a product of $\mathcal{S}_{ss'}$ or $\mathcal{S}_{ss'}^\dagger$ along a sequence of edges.

To determine the self-statistics of $(\mathcal{A}_s, B_s) = (1, -1)$, we make an counterclockwise exchange of two such excitations, named a and b for keeping track of their paths. Initialize a and b at sites 1 and 2 respectively in Fig. S2(a). In terms of the basic moves $M_1 = \mathcal{S}_{14}$ ($4 \rightarrow 1$), $M_2 = \mathcal{S}_{47}^\dagger$ ($4 \rightarrow 7$), and $M_3 = \mathcal{S}_{24}$ ($4 \rightarrow 2$) for this type of excitation, the exchange can be realized as follows: first move a from 1 to 7 by $M_2 M_1^\dagger = \mathcal{S}_{47}^\dagger \mathcal{S}_{14}^\dagger$, then b from 2 to 1 by $M_1 M_3^\dagger = \mathcal{S}_{14} \mathcal{S}_{24}^\dagger$, and finally a from 7 to 2 by $M_1 M_2^\dagger = \mathcal{S}_{24} \mathcal{S}_{47}$. It results in

$$\mathcal{S}_{24} \mathcal{S}_{47} \mathcal{S}_{14} \mathcal{S}_{24}^\dagger \mathcal{S}_{47}^\dagger \mathcal{S}_{14}^\dagger = i. \quad (\text{S19})$$

Namely, $(\mathcal{A}_s, B_s) = (1, -1)$ is a *semion*. In the derivation of Eq. (S19), we used the identities $\mathcal{S}_{24} \mathcal{S}_{47} \mathcal{S}_{14} = -\mathcal{S}_{24} \mathcal{S}_{14} \mathcal{S}_{47} B_4 = -i \mathcal{S}_{14} \mathcal{S}_{24} \mathcal{S}_{47} B_4 = i \mathcal{S}_{14} \mathcal{S}_{47} \mathcal{S}_{24} B_4 = i \mathcal{S}_{14} \mathcal{S}_{47} \mathcal{S}_{24}$, where \mathcal{S}_{24} , \mathcal{S}_{47} , and \mathcal{S}_{14} are permuted by identities (S16) and (S18).

The last excitation type $(\mathcal{A}_s, B_s) = (-1, -1)$ can be viewed as a bound state of $(\mathcal{A}_s, B_s) = (1, -1)$ and $(-1, 1)$. It is created in pairs and moved by $\bar{\mathcal{S}}_{ss'} := \mathcal{S}_{ss'} Z_{ss'}$. Its self-statistics is $-i$, by a computation as in Eq. (S19) but with $\bar{\mathcal{S}}_{ss'}$ used instead.

S.IV. TWISTED CHECKERBOARD MODELS AND THEIR CLASSIFICATION

In this section, we provide some more details about the twisted checkerboard models used in the main text.

A. Construction details of twisted checkerboard models

In this subsection, we explain how the non-Pauli stabilizer formulation is obtained for the seven twisted checkerboard models. The construction is done via the correspondence between the double semion model and each layer of 3D twisted checkerboards as illustrated in Fig. S2, which also motivates the expression of twisted X operators explicitly given in Sec. S.IV B.

On the double semion side, for the model on the 2D checkerboard \mathcal{D} in Fig. S2(a), let $(Z|\mathcal{D})$ denote the configuration of all its qubits in the Z basis. Then \mathcal{A}_s in Eq. (S11) takes the form $\mathcal{A}_s = A_s \phi_s(Z|\mathcal{D})$, where A_s is a product of four Pauli X operators, and $\phi_s(Z|\mathcal{D})$ is a $U(1)$ phase associated with the change of $(Z|\mathcal{D})$ made by A_s . In fact, $\phi_s(Z|\mathcal{D})$ only depends on the Z 's associated with a finite number of qubits near s . Similarly, $\mathcal{S}_{ss'}$ in Eqs. (S12) and (S13) can be viewed as a modified X operator of the form $X_\sigma = X_\sigma \gamma_\sigma(Z|\mathcal{D})$ with $\gamma_\sigma(Z|\mathcal{D}) \in U(1)$, where $\sigma \in \mathcal{D}$ labels qubits.

On the 3D checkerboard side, by a κ -layer we mean a single layer of cubes arranged on a plane perpendicular to the κ -direction, where $\kappa = x, y, z$. The κ -edges within can be labeled by

$$\mathcal{E}_n^\kappa := \{x^{j_x} y^{j_y} z^{j_z} (1 + \kappa) \mid j_\kappa = n\} \quad (\text{S20})$$

for $n \in \mathbb{Z}$. Each layer corresponds to a 2D checkerboard, with \mathcal{E}_n^κ mapped to vertices and gray (blank) cubes to gray (white) squares. The edge variable on $\ell = \nu(1 + \kappa)$ is $Z_\ell := Z_\nu Z_{\nu\kappa}$. Let $(Z|\mathcal{E}_n^\kappa)$ denote the configuration of edge variables Z_ℓ for $\ell \in \mathcal{E}_n^\kappa$. The change of $(Z|\mathcal{E}_n^\kappa)$ under A_c is like that of $(Z|\mathcal{D})$ under some A_s , if c is adjacent to \mathcal{E}_n^κ . We can thus assign a phase $\phi_c(Z|\mathcal{E}_n^\kappa) \in U(1)$ to this change as in the double semion model. We may require $\phi_c(Z|\mathcal{E}_n^\kappa) = 1$ if c is not adjacent to \mathcal{E}_n^κ , for $(Z|\mathcal{E}_n^\kappa)$ is unchanged by A_c in this situation. Similarly, for the change of $(Z|\mathcal{E}_n^\kappa)$ under X_ν , there is a phase $\gamma_\nu(Z|\mathcal{E}_n^\kappa) \in U(1)$ associated analogously as for $\mathcal{S}_{ss'}$ in Eqs. (S12) and (S13).

The twisted checkerboard model H_{cb}^x is obtained by twisting all x -layers, namely,

$$A_c \rightarrow A_c^x = A_c \prod_n \phi_c(Z|\mathcal{E}_n^x) \equiv A_c \Phi_c^x \quad \text{and} \quad X_\nu \rightarrow X_\nu^x = X_\nu \prod_n \gamma_\nu(Z|\mathcal{E}_n^x) \equiv X_\nu \Gamma_\nu^x, \quad (\text{S21})$$

where $\Phi_c^x := \prod_n \phi_c(Z|\mathcal{E}_n^x)$ and $\Gamma_\nu^x := \prod_n \gamma_\nu(Z|\mathcal{E}_n^x)$ for short. For each A_c^x (and X_ν^x), only the two layers adjacent to c (respectively, ν) contribute a nontrivial factor. Moreover, Φ_c^x and Γ_ν^x are local operators. The explicit expressions of A_c^x and X_ν^x are given in the main text and in Sec. S.IV B respectively, obtained based on the correspondence between \mathcal{E}_n^x and \mathcal{D} in Fig. S2(b). The algebraic properties of A_c^x and X_ν^x can be derived analogously as in Sec. S.III. In particular, one has $(A_c^x)^2 = 1$ and $[A_c^x, B_{c'}] = [A_c^x, X_\nu^x] = 0$, which enable us to analyze the model H_{cb}^x as a non-Pauli stabilizer code.

For concreteness, we illustrate how the expression of A_c^x in the main text is obtained. On the double semion side, label the qubits by $\mu^j \nu^k$ as in Fig. S2(a). Then, for example, Z_{13} and Z_{14} are denoted $Z_{\bar{\mu}\nu}$ and Z_ν respectively below. The controlled- Z gate on them can be expressed as

$$C(Z_{13}, Z_{14}) = C(Z_{\bar{\mu}\nu}, Z_\nu) = (-1)^{n_{\bar{\mu}\nu}^- n_\nu^-}, \quad (\text{S22})$$

where $C(\cdot, \cdot)$ is defined by Eq. (S9) and $n_\nu^- := \frac{1}{2}(1 - Z_\nu)$. Similarly, we have $C(Z_{14}, -Z_{24}) = (-1)^{n_{\bar{\mu}\nu}^- n_{\mu\nu}^+}$ with $n_{\mu\nu}^+ := \frac{1}{2}(1 + Z_{\mu\nu})$ etc. Thus, \tilde{A}_4 in Eq. (S8) can be reformulated as

$$\tilde{A}_4 = A_4 (-1)^{n_{\bar{\mu}\nu}^- n_\nu^- + n_{\bar{\mu}\nu}^- n_{\mu\nu}^+ + n_{\mu\nu}^+ n_{\mu^2\nu}^- + n_{\mu^2\nu}^- n_{\bar{\mu}\nu}^- + n_{\bar{\mu}\nu}^- n_{\mu\nu}^+ + n_{\mu\nu}^+ n_{\mu^2\nu}^-} (-1)^{n_{\bar{\mu}\nu(1+\mu)}^- n_{\mu(1+\mu)(1+\nu)}^-} \quad (\text{S23})$$

where $n_{\mu\nu(1+\mu)}^- := \frac{1}{2}(1 - Z_{\mu\nu(1+\mu)})$ with $Z_{\mu\nu(1+\mu)} := Z_{\mu\nu} Z_{\mu^2\nu}$ and in general $n_\kappa^\pm := \frac{1}{2}(1 \pm Z_\kappa)$ with $Z_\kappa := \prod_{\nu \in \kappa} Z_\nu$ for any finite set κ of qubits. Moreover, \mathcal{A}_4 in Eq. (S8) takes the form

$$\mathcal{A}_4 = A_4 (-1)^{n_{\bar{\mu}\nu}^- n_{\bar{\mu}\nu}^- + n_{\bar{\mu}\nu}^- n_\nu^- + n_{\bar{\mu}\nu}^- n_{\mu\nu}^+ + n_{\mu\nu}^+ n_{\mu^2\nu}^- + n_{\mu^2\nu}^- n_{\bar{\mu}\nu}^- + n_{\bar{\mu}\nu}^- n_{\mu\nu}^+ + n_{\mu\nu}^+ n_{\mu^2\nu}^-} \cdot (-1)^{n_{\bar{\mu}\nu(1+\mu)}^- n_{\mu(1+\mu)(1+\nu)}^-} \cdot t_{\bar{\mu}(1+\bar{\nu})(1+\nu)}^-, \quad (\text{S24})$$

Based on the correspondence between \mathcal{E}_n^x and \mathcal{D} in Fig. S2(b), A_c^x in the twisted checkerboard model H_{cb}^x can be expressed as $A_c^x = A_c \Phi_c^x = A_c \phi_{(1+x)\bar{x}c} \phi_{(1+x)xc}$, where $\phi_{(1+x)\bar{x}c}$ and $\phi_{(1+x)xc}$ denote the twisting factors associated with the x -layers containing x -edges whose vertices are $\ell = (1+x)\bar{x}c$ and $\ell = (1+x)xc$ respectively. Explicitly,

$$\phi_\ell := (-1)^{n_{\bar{y}\bar{z}}^- n_{\bar{y}z}^- + n_{\bar{y}z}^- n_{\bar{y}\bar{z}}^- + n_{\bar{y}\bar{z}}^- n_{\bar{y}z}^- + n_{\bar{y}z}^- n_{\bar{y}\bar{z}}^-} \cdot (-1)^{n_{\bar{y}z(1+y)}^- n_{\bar{y}(1+y)(1+z)}^-} \cdot t_{\bar{\ell}(1+\bar{y})(1+z)}^-, \quad (\text{S25})$$

which is obtained from the twisting factor of Eq. (S24) by replacing Z_v (which appears in $n_v^\pm := \frac{1}{2}(1 \pm Z_v)$) etc) with edge variable, e.g., $Z_{\ell v} = Z_{\bar{x}c} Z_{c v}$ for $\ell = (1+x)\bar{x}c$. As illustrated in Fig. S2(b), for $c = 1$ (the dashed magenta cube), $\phi_{(1+x)\bar{x}c}$ is associated with the x -edges of the two darker gray cubes.

Twisting factors $\Phi_c^y, \Gamma_v^y, \Phi_c^z,$ and Γ_v^z along y -layers and z -layers are obtained from Φ_c^x and Γ_v^x by the 3-fold rotation that permutes $x, y,$ and z directions. They are used in defining the remaining twisted checkerboard models mentioned in the main text. For instance, H_{cb}^{xy} is obtained by the replacement $A_c \rightarrow A_c^{xy} = A_c \Phi_c^x \Phi_c^y$.

Note that one may obtain different twisting factors if \mathcal{E}_n^μ with \mathcal{D} are matched in a different way, but this will not result in new phases. As an illustration, let $\bar{\Phi}_c^y$ and $\bar{\Gamma}_v^y$ denote the twisting factors obtained from the \mathcal{E}_n^μ - \mathcal{D} correspondence in Fig. S2(c), where \bar{y} refers to $\hat{\mu} \times \hat{\nu} = -\hat{y}$. Although $\bar{\Phi}_c^y \neq \Phi_c^y$, the change of \mathcal{E}_n^μ - \mathcal{D} correspondence is equivalent to a retriangulation of \mathcal{D} and hence, as in 2D [53], we may use a Pachner-move-motivated local unitary transformation to identify the corresponding quantum phases.

B. Two derivations of semionic fracton self-statistics

In this subsection, two derivations are given to show that the B excitation of H_{cb}^x , denoted m_x , is a semionic fracton.

One approach is to work out the details of the twisted X operator for generating fractional moves of B excitations explicitly. First, using Eq. (S21) and the \mathcal{E}_n^μ - \mathcal{D} correspondence in Fig. S2(b), we obtain

$$X_v^x = X_v \varphi_{(1+\bar{x})v} \varphi_{(1+\bar{x})xv}, \quad (\text{S26})$$

where $(1+\bar{x})v$ and $(1+\bar{x})xv$ correspond to the two x -edges connecting to v . For ℓ ($\bar{\ell}$) of the form $(1+\bar{x})x^j y^k z^l$ with $j+k+l$ even (odd),

$$\varphi_\ell := i^{-n_{\bar{y}v}^-} (-1)^{n_{\bar{y}v}^- + n_{\ell+\bar{y}v}^+ + n_{\ell+\bar{y}v}^- + n_{\ell+\bar{y}v}^+} (-1)^{n_{\ell+\bar{y}v}^-}, \quad (\text{S27})$$

$$\varphi_{\bar{\ell}} := i^{n_{\bar{y}v}^-} (-1)^{n_{\bar{y}v}^- + n_{\ell+\bar{y}v}^+ + n_{\ell+\bar{y}v}^- + n_{\ell+\bar{y}v}^+} (-1)^{n_{\ell+\bar{y}v}^-}, \quad (\text{S28})$$

where $n_\kappa^\pm := \frac{1}{2}(1 \pm Z_\kappa)$ with $Z_\kappa := \prod_{v \in \kappa} Z_v$ for any finite set of vertices κ (written as a formal sum). The commutation relation

$$X_v^x X_{v'}^x = \begin{cases} X_v^x X_{v'}^x \prod_{c \ni v, v'} B_c, & v' v^{-1} \notin xy\text{-plane}, \\ (-1)^v i X_v^x X_{v'}^x, & v' v^{-1} = xy, x\bar{y}, \\ -(-1)^v i X_v^x X_{v'}^x, & v' v^{-1} = \bar{x}y, \bar{x}\bar{y}, \\ X_v^x X_{v'}^x, & \text{otherwise} \end{cases} \quad (\text{S29})$$

can be established by direct computation, where $c \ni v, v'$ labels colored cubes which contain both v and v' , and $(-1)^v := (-1)^{j+k+l}$ for $v = x^j y^k z^l$. In addition, we have $(X_v^x)^2 = \prod_{c \ni v} B_c$ and hence $X_v^{x\dagger} = X_v^x \prod_{c \ni v} B_c$. One can use X_v^x to flip the four B_c terms on the cubes connecting to v . This generates fractional moves for windmill processes explicitly. For m_x (i.e., a $B_c = -1$ excitation of H_{cb}^x), utilizing Eq. (S29), we obtain

$$\theta_{m^x}^{[xyz]} = \theta_{m^x}^{[x\bar{y}\bar{z}]} = i \quad \text{and} \quad \theta_{m^x}^{[\bar{x}y\bar{z}]} = \theta_{m^x}^{[\bar{x}\bar{y}z]} = -i \quad (\text{S30})$$

by a straightforward computation.

The second approach provides a fast and intuitive way to write down fracton self-statistics in twisted models. In this approach, to get the self-statistics of m_x in H_{cb} , we consider another model h_{cb}^x obtained by twisting the checkerboard model along x -layers only in the $x > 0$ region. Let b_\pm denote one $B_c = -1$ excitation of h_{cb}^x at $\pm(l, l, l)$ for $l > 0$. Since h_{cb}^x is twisted as H_{cb}^x for $x > 0$ and untwisted for the $x < 0$ region, b_+ has the same self-statistics as m_x in H_{cb}^x and meanwhile b_- has purely bosonic self-statistics. Moreover, note that both $S_{b_+ b_-}^\mu$ and $S_{b_- b_+}^\mu$ are trivial for $\mu = x, y, z$. Hence we get $\theta_{b_+ \times b_-}^{[\tau]} = \theta_{b_- \times b_+}^{[\tau]}$ by Eq. (S6) (i.e., Eq. (6) of the main text) for $\tau = xyz$, and analogously also the correspondents for $\tau = \bar{x}\bar{y}z, x\bar{y}\bar{z},$ and $\bar{x}y\bar{z}$. Altogether, we have

$$\theta_{m^x}^{[\tau]} = \theta_{b_+}^{[\tau]} = \theta_{b_+ \times b_-}^{[\tau]} \quad (\text{S31})$$

for $\tau = xyz, \bar{x}\bar{y}z, x\bar{y}\bar{z},$ and $\bar{x}y\bar{z}$. This greatly simplifies the computation of $\theta_{m^x}^{[\tau]}$ because $b_+ \times b_-$ is reducible into three dipolar planons (analogous to those in Eq. (S3)). In h_{cb}^x , one of the planons is semionic, which implies Eq. (S30) immediately by using Eq. (S31). The idea of the second approach, which simplifies the computation of a fracton's statistics by combining of twisted and untwisted phases, applies to other twisted models of foliated fractons.

C. Classification of twisted checkerboard models

In this subsection, we show how local unitary transformations can be obtained for establishing the classification, claimed in the main text, of twisted fraction models. Recall that two gapped models belong to the same phase if and only if their ground states are related by a local unitary transformation [56].

Let us illustrate this by explaining how to find a local unitary transformation connecting H_{cb}^{xy} and H_{cb} . For convenience, we use the \mathcal{E}_n^x - \mathcal{D} and \mathcal{E}_n^y - \mathcal{D} correspondences in Figs. S2(b) and (c) for twisting construction. Denote the corresponding model by H_{cb}^{xy} . As discussed in the last paragraph of Sec. S.IV A, it only differs from H_{cb}^{xy} by a local unitary transformation. For H_{cb}^{xy} , the twisted X operator takes the form $X_v^{xy} = X_v \Gamma_v^x \Gamma_v^y$, where Γ_v^x and Γ_v^y are related by the reflection that swaps x and y . By analogy to the commutation relation of X_v^x in Eq. (S29), one has that X_v^{xy} and $X_{v'}^{xy}$ anticommute for $v' = (xy)^{\pm 1} v$ and commute otherwise. Therefore, the operator $\mathcal{X}_v := X_v^{xy} Z_{xyv}$ has the same algebraic properties as X_v . Hence there should exist a local unitary transformation U that maps X_v to \mathcal{X}_v while keeping Z_v fixed.

Working out the details explicitly, we have

$$\mathcal{X}_v := X_v^{xy} Z_{xyv} = X_v i^{(-1)^v (n_{xy}^- + n_{xy}^-)} (-1)^{n_{xy}^- n_{xy}^- + n_{xy}^- n_{xy}^- + n_{xy}^- n_{xy}^- + n_{xy}^- n_{xy}^- + n_{xy}^- n_{xy}^- + n_{xy}^- n_{xy}^- + n_{xy}^- n_{xy}^- + n_{xy}^- n_{xy}^-}. \quad (\text{S32})$$

It implies that the transformation $X_v \mapsto \mathcal{X}_v$ can be realized by the local unitary

$$U := \prod_v i^{(-1)^v n_{xy}^- n_{xy}^-} (-1)^{n_{xy}^- n_{xy}^- + n_{xy}^- n_{xy}^-}. \quad (\text{S33})$$

Furthermore, by a straightforward but tedious calculation, we can show $U H_{\text{cb}} U^\dagger \simeq H_{\text{cb}}^{xy}$, where \simeq means that two operators acting identically on states satisfying $B_c = 1, \forall c$. Thus, the ground states of H_{cb} , H_{cb}^{xy} , and hence also H_{cb}^{xy} are related by local unitary transformations. They all belong to the same fracton phase.

Remarkably, by the above discussion, we proved that twistings in two different directions are related and can even cancel each other through a local unitary transformation. For us, this fact was so counterintuitive initially that we did not even think that it could be true until we calculated the fracton self-statistics. Combined with this fact, the presence and absence of semionic fracton indeed yields the classification stated in the main text about twisted checkerboard models.

S.V. MOBILITY CONES

In this section, we provide a mathematical treatment of *mobility cones*, together with necessary preliminaries.

A. Mathematical preliminaries

Definition 1. A set $K \subseteq \mathbb{R}^d$ is called a *cone* if $\alpha v \in K, \forall v \in K, \forall \alpha \in \mathbb{R}_{\geq 0}$.

Definition 2. A cone $K \subseteq \mathbb{R}^d$ is called *convex* if $\alpha_1 v_1 + \alpha_2 v_2 \in K, \forall v_1, v_2 \in K, \forall \alpha_1, \alpha_2 \in \mathbb{R}_{\geq 0}$.

Definition 3. Given a set $S \subseteq \mathbb{R}^d$, the *conical hull* of S is denoted $\text{cone}(S)$ and defined as

$$\text{cone}(S) := \left\{ \sum_{j=1}^n \alpha_j v_j \mid v_j \in S, 0 \leq \alpha_j \in \mathbb{R}, j, n \in \mathbb{N} \right\}. \quad (\text{S34})$$

For $S = \emptyset$, $\text{cone}(S) := \{\mathbf{0}\}$. Each element of $\text{cone}(S)$ is called a *conical combination* of S .

Remark 1. It is clear that $\text{cone}(S)$ is a convex cone. Actually, $\text{cone}(S)$ is the smallest convex cone containing S .

The above basic definitions about convex cones may be found in the mathematical literature, e.g., Ref. [57].

B. Definition of mobility cones

We now define the notion of *mobility cones* for quasiparticles (especially for fractons) in a gapped phase. Let \mathbb{E}^3 be the Euclidean space where physical degrees of freedom live. We view \mathbb{R}^3 as the group of translations. For $K \subseteq \mathbb{R}^3$ and $\mathcal{C} \subseteq \mathbb{E}^3$, let

$$\mathcal{C} + K := \{x + v \mid x \in \mathcal{C}, v \in K\} \subseteq \mathbb{E}^3. \quad (\text{S35})$$

Let q denote a quasiparticle superselection sector (i.e., a particle type up to local operations).

Definition 4. A closed convex cone $K \subseteq \mathbb{R}^3$ is called a *mobility cone* for q (and any quasiparticle in this superselection sector) if there exists a finite region $\mathcal{C} \subseteq \mathbb{E}^3$ such that q can be realized by excitations supported inside $(\mathcal{C} + K) \setminus (-n, n)^3$, $\forall n \in \mathbb{N}$, where $(-n, n)^3$ denotes a cube centered at the origin and $(\mathcal{C} + K) \setminus (-n, n)^3$ is a region with $(-n, n)^3$ excluded.

Physically, this means that quasiparticles in the sector q can move (probably in a fractional way) to infinity within the conical region $\mathcal{C} + K$.

Example 1. The empty set $K = \emptyset$ is a mobility cone for q if and only if q is the trivial superselection sector. Note $\mathcal{C} + K = \emptyset$ and $(\mathcal{C} + K) \setminus (-n, n)^3 = \emptyset$ if $K = \emptyset$. A state with excitations supported inside $(\mathcal{C} + K) \setminus (-n, n)^3 = \emptyset$ simply contains no excitation at all.

Example 2. Both cone (\hat{x}) and $-\text{cone}(\hat{x})$ are mobility cones for a quasiparticle with conventional mobility along the \hat{x} -direction.

Example 3. Fractons do not have conventional mobility along any direction. Hence they allow only two- or three-dimensional mobility cones. Besides, a pair of cones related by inversion, $\pm K$, do not have to be both mobility cones for a fracton superselection sector, as we have noticed in the Haah's code.

C. Invariance of mobility cone under local unitary

Suppose that H is a gapped Hamiltonian and U a local unitary. Each superselection sector q of H is then mapped by U to a superselection sector \tilde{q} of UHU^\dagger . If K is a mobility cone for q , it is clear that K is also a mobility cone for \tilde{q} .

D. Mobility cones in Haah's code

Consider the Haah's code H_{Haah} . Denote the lattice translation group by $\Lambda := \{x^i y^j z^k | i, j, k \in \mathbb{Z}\}$. Let $R := \mathbb{Z}_2 \Lambda$ be the group ring of Λ over $\mathbb{Z}_2 = \{0, 1\}$. The elements of R can be thought as Laurent polynomials in x, y , and z .

For H_{Haah} , excitation patterns within finite regions are labeled by $(a, b) \in R^2$ with a and b specifying the configurations of the A -term and B -term excitations respectively. Two excitation patterns (a, b) and (a', b') belong to the same superselection sector, and we write $(a, b) \sim (a', b')$, if and only if $a - a' \in I$ and $b - b' \in \bar{I}$, where

$$I \equiv (f_1, f_2)_R := \{a_1 f_1 + a_2 f_2 | a_1, a_2 \in R\} \quad \text{and} \quad \bar{I} \equiv (\bar{f}_1, \bar{f}_2)_R := \{a_1 \bar{f}_1 + a_2 \bar{f}_2 | a_1, a_2 \in R\} \quad (\text{S36})$$

are two ideals of R , and we remind the reader that $f_1 = 1 + x + y + z$ and $f_2 = 1 + xy + xz + yz$. Thus, superselection sectors can be labeled by $(R/I) \times (R/\bar{I})$, where R/I and R/\bar{I} denote quotient rings.

In particular, $(a, b) \sim (0, 0)$ and represents the trivial superselection sector if and only if $a \in I$ and $b \in \bar{I}$. All the *nontrivial* superselection sectors are fractonic and can be put into three groups: type- A , type- B , and mixed.

Definition 5. A nontrivial superselection sector $(q_A, q_B) \in (R/I) \times (R/\bar{I})$ is called *type- A* (respectively, *type- B*) if $q_B = 0$ (respectively, $q_A = 0$). It is called *mixed* if $q_A \neq 0$ and $q_B \neq 0$.

The ideal $I \equiv (f_1, f_2)_R$ describes the fractional moves of A -term excitations. It can also be generated by f_1 and $g = (y + z)f_1 + f_2 = z^2 + (y + 1)y + y^2 + y + 1$. Namely, the ideal $(f_1, g)_R := \{a_1 f_1 + a_2 g | a_1, a_2 \in R\}$ is identical to $(f_1, f_2)_R$. From g , it is clear that

$$K_1 := \text{cone}(\hat{y}, \hat{z}), \quad K_2 := \text{cone}(\hat{z} - \hat{y}, -\hat{y}), \quad K_3 := \text{cone}(-\hat{z}, \hat{y} - \hat{z}) \quad (\text{S37})$$

are 2D mobility cones for all type- A superselection sectors. Their spatial inversions $-K_1$, $-K_2$, and $-K_3$ are mobility cones for all type- B superselection sectors. See Fig. 5 of the main text for a visual. In general, one may also consider 3D mobility cones, like cone $(\hat{x} + \hat{y}, \hat{y} + \hat{z}, \hat{z} + \hat{x})$ for type- A superselection sector (as implied by $f_2 = 1 + xy + yz + zx$). Nevertheless, for simplicity, we focus on 2D mobility cones along the yz plane, which suffice for our current purpose.

To confirm that type- A and type- B can be distinguished by mobility cones, we show that none of $-K_i$'s (respectively, K_i 's) is a mobility cone of any type- A (respectively, type- B) superselection sector. Note that it is possible to permute the three K_i 's while keeping $I = (f_1, g)_R$ invariant using two transformations (1) a swap $y \leftrightarrow z$ and (2) a mapping given by $x \mapsto x\bar{z}$, $y \mapsto y\bar{z}$, and $z \mapsto \bar{z}$. Hence we only need to consider one of K_i 's (e.g., K_3). See below.

Claim 1. The cone $-K_3$ is not a mobility cone for any type- A superselection sector.

Proof. Argue by contradiction. Assume that $-K_3$ is a mobility cone for type- A superselection sector $(q_A, 0)$. Then there exists $\xi_n \in q_A$ supported inside $(\mathcal{C} - K_3) \setminus (-n, n)^3$, $\forall n \in \mathbb{N}$. Note $-K_3 = \text{cone}(\hat{z}, \hat{z} - \hat{y})$. By using translation symmetry and the modulo operations of first f_1 and then g , we can reduce ξ_n to be of the form $\xi_n = (\xi'_n z + \xi''_n) z^n$ where ξ'_n and ξ''_n are arbitrary Laurent polynomials in y . Let $\deg(\xi_n)$ denote the highest total degree of ξ_n , and $\deg_-^y(\xi_n)$ denote the lowest degree of ξ_n in y . For example, $\deg(\bar{y}z + 1) = 0$ and $\deg_-^y(\bar{y}z + 1) = -1$. Note $\deg(\xi_n) - \deg_-^y(\xi_n) \geq n$. Moreover, $\xi_n \equiv \xi_{n-1} \pmod{I}$ implies $\deg(\xi_n) = \deg(\xi_{n-1})$ and $\deg_-^y(\xi_n) = \deg_-^y(\xi_{n-1})$, which can be checked straightforwardly. Hence, we have $\deg(\xi_0) - \deg_-^y(\xi_0) = \deg(\xi_n) - \deg_-^y(\xi_n) \geq n, \forall n \in \mathbb{N}$. This contradicts the fact that ξ_0 is an excitation configuration inside a finite region, proving the claim. \square

Therefore, $-K_i$'s (respectively, K_i 's) are not mobility cones for type- A (respectively, type- B) superselection sector. Moreover, K_i 's and $-K_i$'s have to be combined to provide a mobility cone for each mixed superselection sector. This is how type- A , type- B , and mixed superselection sectors are distinguished in the main text.

S.VI. TWISTED HAAH'S CODE

This section presents details of the spin model for twisted Haah's code [38]. It is explicitly defined by the Hamiltonian

$$H_{\text{Haah}}^F = - \sum_{\lambda} (A_{\lambda} + \tilde{B}_{\lambda}), \quad (\text{S38})$$

which is obtained by replacing the B -term of the original Haah's code H_{Haah} with

$$\tilde{B}_{\lambda} = (t_1 f_2, t_2 f_1, f_2, f_1), \quad (\text{S39})$$

where $t_1 = x + y + z + \bar{x}y + \bar{y}z + \bar{z}x$ and $t_2 = xy + yz + zx + \bar{x}y + \bar{y}z + \bar{z}x$.

The twisted model is designed such that it gives rise to an emergent H_{Haah} -governed fermionic gauge theory. This is mentioned in the main text and can be understood using the exact correspondence of degrees of freedom [21]

$$X_{\sigma} \mapsto X_{\sigma} \quad \text{and} \quad Z_{\sigma} c_{\sigma} \mapsto Z_{\sigma} T_{\sigma} \quad (\text{S40})$$

between the gauge theory and the spin model, where c_{σ} is a product of Majorana operators, as defined in the main text, and T_{σ} is a product of Pauli X 's which correspond to the t factors in Eq. (S39). In the construction, the exact form T_{σ} and t factors are specified by the requirement that (anti)commutation relations should be preserved during the correspondence.

S.VII. DISCRETENESS OF FRACTON SELF-STATISTICS IN THE HAAH'S CODE AND ITS TWISTED VARIANT

In this section, we examine in greater detail the A -excitation self-statistics described in the main text for the Haah's code and its twisted variant. We show that it allows only two discrete values ± 1 for both phases.

Consider the exchange process $\theta_a = M_3^{\dagger} M_2 M_1^{\dagger} M_3 M_2^{\dagger} M_1$ of A -excitations a (initialized at the origin $x^0 y^0 z^0 \equiv 1$) and \widehat{a} (initialized at η_2) in the Haah's code or its twisted variant, where $M_i : 1 \rightarrow \eta_i$ for $i = 1, 2, 3$ are fractional moves along the yz -plane with η_i located as in Fig. S3. Making the exchange twice gives

$$\theta_a^2 = M_3^{\dagger} (M_2 M_1^{\dagger}) M_3 M_2^{\dagger} (M_1 M_3^{\dagger}) M_2 M_1^{\dagger} (M_3 M_2^{\dagger}) M_1, \quad (\text{S41})$$

where parentheses are inserted to notionally separate the moves of \widehat{a} from those of a . Note that $f_1 = 1 + x + y + z$ gives a fractional move $1 \rightarrow 1 + \bar{x}f_1 = (1 + y + z)\bar{x}$. It can be iterated to generate fractional moves of each A -excitation, along a cyan tetrahedron illustrated in Fig. S3, from the yz -plane (i.e., $x = 0$) to any $x = -n$ plane for $n = 1, 2, 3 \dots$. Thus, we have $\eta_i \rightarrow \eta_i (\bar{x} + \bar{x}y + \bar{x}z) \rightarrow \eta_i (\bar{x} + \bar{x}y + \bar{x}z)^2 \rightarrow \dots \rightarrow \eta_i (\bar{x} + \bar{x}y + \bar{x}z)^n$. Together with the inverse of $\eta_j \rightarrow \eta_j (\bar{x} + \bar{x}y + \bar{x}z)^n$, we can deform the moves $M_j M_i^{\dagger} : \eta_i \rightarrow 1 \rightarrow \eta_j$ for \widehat{a} into

$$N_{ji} : \eta_i \rightarrow \eta_i (\bar{x} + \bar{x}y + \bar{x}z)^n \rightarrow (\bar{x} + \bar{x}y + \bar{x}z)^n \rightarrow \eta_j (\bar{x} + \bar{x}y + \bar{x}z)^n \rightarrow \eta_j \quad (\text{S42})$$

to bypass the origin, where $\eta_i (\bar{x} + \bar{x}y + \bar{x}z)^n \rightarrow (\bar{x} + \bar{x}y + \bar{x}z)^n \rightarrow \eta_j (\bar{x} + \bar{x}y + \bar{x}z)^n$ is the analogue of $\eta_i \rightarrow 1 \rightarrow \eta_j$ but realized on the $x = -n$ plane. Using the original paths M_i for a and the detoured paths N_{ji} for \widehat{a} , we can deform θ_a^2 (Eq. (S41)) into a trivial process. Thus, $\theta_a^2 = 1$ and hence $\theta_a = \pm 1$.

Actually, the above argument for $\theta_a = \pm 1$ holds as long as a allows a mobility cone out of the plane where θ_a is realized. The discreteness of θ_a justifies its use in distinguishing fracton orders.

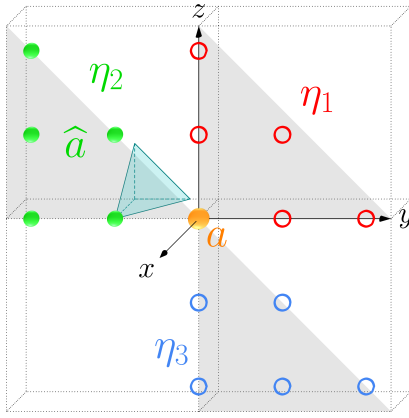


Figure S3. A state with A -excitations a (at the origin) and \hat{a} (at η_2) in the Haah's code or its twisted variant. Each A -excitation can be moved along a tetrahedron (like the cyan one) towards where $x = -n$ plane, where n can be $1, 2, 3, \dots$.